RSC Advances

PAPER

View Article Online
View Journal | View Issue

Cite this: *RSC Adv.*, 2023, **13**, 1216

Preparation of a $Bi_6O_5(OH)_3(NO_3)_5 \cdot 2H_2O$/AgBr composite and its long-lasting antibacterial efficacy†

Mei Zhao, *[a] Mengchen Liu,[a] Jinfeng Yao,[a] Wenyu Li,[a] Chengdong Li,[a] Qian Zhang,[a] Zhihua Zhang[b] and Wenjun Wang[c]

A novel $Bi_6O_5(OH)_3(NO_3)_5 \cdot 2H_2O$/AgBr (6535BBN/AgBr) composite with long-lasting antibacterial efficacy was prepared. The microstructure of the composite was characterized. AgBr nanoparticles (NPs) were sandwiched in 6535BBN nanosheets (NSs) or loaded on their surfaces. The utilization of 6535BBN as carriers contributed to the long-term lasting antibacterial activity of the composite after storage in water or 0.9% NaCl. The antibacterial activity was evaluated by inhibition zones against *E. coli*. The inhibition zone diameters of 6535BBN/AgBr stored in water for 0 h, 8 h, 16 h, and 48 h were measured as 22.50, 21.71, 20.43, and 20.29 mm, respectively. The activity of the composite after storage in water for 48 h remained 90.2% of that in the beginning. After storing in 0.9% NaCl for 16 h, the activity was determined to be 90.1% of that in the beginning. In comparison with the rapid decrease in the antibacterial activity of pure AgBr, the slow reduction of 6535BBN/AgBr after storage indicates long-lasting efficacy. The excellent dispersion states of 6535BBN/AgBr powders after storage in solutions were revealed, and the positive relationship between the dispersion state and its long-lasting antibacterial activity was suggested. Based on the unique load-on-carrier (LOC) structure, the long-lasting antibacterial performance was promoted by the synergy of the sharp-edge-cutting effect of 6535BBN NSs, prolonged ROS antibacterial effect, and restrained sterilization effects of silver ions caused by their slow release.

Received 23rd November 2022
Accepted 15th December 2022

DOI: 10.1039/d2ra07447h

rsc.li/rsc-advances

Introduction

The antibiotic resistance of bacteria and the corresponding excessive use of antibiotics had caused a rapid increase of drug-resistant pathogens and antibiotic contamination in the aqueous environment.[1–3] It is urgent to develop long-lasting antibacterial efficacy and explore non-drug antibacterial nanomaterials. The long-term lasting antibacterial effect means the antibacterial activity of materials stored in solution for a certain period, which is vitally significant for clinical applications because some infections might occur throughout the entire treatment period such as the implant infection in implantation operations.[4–8] Non-drug antibacterial nanomaterials have attracted increasing attention because of their promising antibacterial and antimicrobial capacities, for example, Ag, Au, and TiO_2 nanoparticles (NPs).[9–11] Some non-drug nanomaterials have exhibited effective long-lasting antibacterial performance and potential value in clinical treatments, for example, Cu/Ti–6Al–4V, Cu/GO, and polylactic acid (PLLA)/Ag.[8,12,13] In 2020, Liu *et al.* successfully synthesized the "inside–outside" Ag-NPs-loaded composite fibers, and Ag-NPs were uniformly distributed on the inner surface of the PLLA fibers. The beneficial LOC structure endowed the PLLA/Ag composite with good physiological stability, long-term antibacterial effect, and bone infection inhibition ability and made it a promising bone implant material.[13]

Silver halides (AgX, X = Cl, Br, I) have been accepted as non-drug antibacterial materials due to photocatalytic ROS antibacterial actions and sterilization effects of silver ions.[14–16] However, the instability and photosensitivity are the practical limits for clinical applications.[17–19] The instability of AgX includes the tendency to decompose and aggregate in the biological media, leading to the failure of the remaining stable dispersion in solutions.[17,18] As a result, the antibacterial capacity of AgX deteriorates even after a short time. Some researchers have tried to prepare AgX composites with the LOC microstructure, where AgX NPs with decreased size were loaded on suitable carrier materials.[20–22] They indicated that the LOC structure enhanced the stability of AgX NPs and protected them

[a]*College of Materials Science and Engineering, Qingdao University of Science and Technology, Qingdao 266042, China*

[b]*School of Materials Science and Engineering, Dalian Jiaotong University, Dalian 116028, China*

[c]*Research & Development Center for Functional Crystals, Beijing National Laboratory for Condensed Matter Physics, Institute of Physics, Chinese Academy of Sciences, Beijing 100190, China*

† Electronic supplementary information (ESI) available. See DOI: https://doi.org/10.1039/d2ra07447h

from aggregation, which contributed to their antibacterial performances. For example, the AgCl/$ZnWO_4$ composite material displayed excellent antibacterial activity due to its LOC structure, where AgCl NPs were decorated on the $ZnWO_4$ nanorods.[20] As a conclusion, carrier materials with a layered structure played significant roles to improve the antibacterial activity, including C_3N_4, diatomite, and rGO.[23–25] Moreover, prolonging the antibacterial effect by employing suitable layer-structured materials as carriers is promising.

As a group of layer-structured nanomaterials, Bi-based materials, including γ-Bi_2O_3, BiOCl, Bi_2WO_6, $Bi(NO_3)_3$, and BiOI, have exhibited prominent antibacterial performance.[26–30] Basic bismuth nitrate (BBN) consisted of nitrate anions, water molecules, and cage-like $Bi_6O_{4+x}(OH)_{4-x6-x}$, which includes over 15 compounds with different chemical compositions.[31] Some researchers reported the attractive adsorption and photocatalytic performance of some of these BBN compounds.[32–34] However, the antibacterial ability of BBN compounds has scarcely been studied except a few reports and practical usages.[35–37] For example, BBNs are used as milds antiseptic in medicine due to their inhibition against enzymes in bacteria.[35] Bismuth basic nitrate tablet is utilized for the treatment in peptic ulcer because of its antibacterial activity against *H. pylori*.[36,37] In our previous studies, the antibacterial activity and photocatalytic performance of BBN composites were evaluated.[38,39] For tens of BBN compounds, due to their unique layer structure, intrinsic antibacterial activity, and physical and chemical stabilities, it is a good opportunity to be employed as carriers for AgX loading to prolong its antibacterial efficacy.

In this study, one of the BBN compounds, $Bi_6O_5(OH)_3(NO_3)_5 \cdot 2H_2O$ (6535BBN), was utilized as carriers to support AgBr NPs. The typical LOC structure is helpful to enhance the stability of AgBr NPs and protecting them from aggregation, which prolongs the antibacterial efficacy of as-prepared 6535BBN/AgBr composite. To evaluate the long-lasting efficacy, the antibacterial activities of the composite after storage in water or 0.9% NaCl for different durations were measured. The variation of antibacterial activities with the storage time is represented by corresponding inhibition zones against *E. coli*. The dispersion states of 6535BBN/AgBr powders in water or 0.9% NaCl are observed. The mechanism of the long-lasting antibacterial activity is discussed based on the LOC structure. The 6535BBN/AgBr composite and its long-lasting antibacterial efficacy are reported for the first time.

Experimental section

Synthesis

All chemicals were purchased from Sinopharm Chemical Reagent Co. Ltd. The chemicals were of analytical grade and used without further purification. In a typical synthesis, Bi_2O_3 and $AgNO_3$ were used as raw materials. BiOBr was prepared and used as an intermediate product. BiOBr was synthesized as follows. 0.02 mol Bi_2O_3 was added into 40 mL hydrobromic acid at a speed of 3 mL min^{-1} and the solution was magnetically stirred for 30 min. To adjust the pH value to 6, ammonia was added into the solution dropwise. The suspension was magnetically stirred again for 30 min at 40 °C until a light yellow colloid was formed. The colloid was centrifuged and washed with deionized water and alcohol three times. The as-obtained precipitate was dried at 40 °C for 24 h. Thus, the intermediate product BiOBr was prepared. For the typical synthesis of 6535BBN/AgBr, 0.4 g BiOBr was added into 40 mL ethylene glycol and stirred for 30 min. 0.2 g $AgNO_3$ was added into 40 mL ethylene glycol and stirred for 30 min. According to a typical proportion, 0.27 g BiOBr and $AgNO_3$ solutions were mixed together, and the mixed solution was continually stirred for 30 min. 0.49 g polyvinyl pyrrolidone was added into the mixture dropwise. The final solution was continually stirred for 2 h. After then, the final solution was transferred into a Teflon-sealed autoclave and kept at 150 °C for 24 h. The final precipitate was centrifuged, washed with deionized water and ethanol three times, and then dried at 50 °C for 16 h. Finally, a yellowish grey powder was collected for characterization and testing.

Characterization

The formation of the 6535BBN/AgBr composite was confirmed by a Rigaku D/Max 2200 X-ray diffractometer (XRD) with Cu Kα radiation ($\lambda = 1.5406$ Å). The microstructure and composition of the composite were characterized by transmission electron microscopy (TEM, JEM-2100), selected-area electron diffraction (SAED), and energy dispersive spectroscopy (EDS). The elemental composition and chemical state of the composite were analyzed by an X-ray photoelectron spectrometer (XPS, ESCALAB 250Xi). The functional groups on the surface of the as-prepared composite were determined by a NICOLET 5700 FT-IR spectrometer in the range of 500–3600 cm^{-1}.

Evaluation of long-lasting antibacterial activity

The long-lasting antibacterial efficacy of the as-prepared 6535BBN/AgBr and commercial AgBr after storage was evaluated by the disc diffusion method against *E. coli*. Firstly, samples were stored in pure water or 0.9% NaCl for different durations. The as-prepared 6535BBN/AgBr and commercial AgBr were dispersed in water with a concentration of 1 mg mL^{-1}. The tubes were kept without shaking for 0 h, 8 h, 16 h, and 48 h. Similarly, the two samples were stored in 0.9% NaCl for 0 h, 8 h, and 16 h. Secondly, the antibacterial activities of the samples after storage for different durations were evaluated. The glassware used and culture medium were sterilized by autoclaving at 121 °C for 15 min. All experiments were carried out under sterile conditions. Each filter paper disc with a diameter of 6 mm contained 10 μg samples. Distilled water was considered as the negative control. 20 mL agar culture medium was poured into Petri dishes to prepare agar plates. 100 μL bacteria (approximate 1×10^6 colony forming unit (cfu) per mL) were spread evenly on the surface of agar plates. Next, filter papers were placed on the solid culture medium. The culture medium was incubated at 37 °C for 24 h. The diameters of the inhibition zones were measured to evaluate the antibacterial activity. The long-lasting antibacterial efficacy of the as-prepared 6535BBN/AgBr was indicated by the change in the

inhibition zone diameters of the samples after storage in water and 0.9% NaCl for different time durations.

Results and discussion

Phase determination

The crystalline phases of the as-prepared samples were determined by XRD analyses. The spectra in Fig. 1(a) and (b) correspond to the intermediate and final products, respectively. As shown Fig. 1(a), all the diffraction peaks are indexed to tetragonal BiOBr (JCPDS no. 09-0393), which indicates that pure BiOBr with highly crystalline nature is prepared at the first stage. As shown in Fig. 1(b), the diffraction peaks at 30.92°, 44.32°, 55.02°, 64.48°, and 73.20° are assigned to cubic AgBr (JCPDS no. 06-0438), as denoted by black dots. Other peaks at 11.60°, 23.38°, and 26.58° are indexed to rhombohedral $Bi_6O_5(OH)_3(NO_3)_5\cdot 2H_2O$ (JCPDS no. 54-0627). Besides that, no other diffraction peak is observed. Based on the above XRD results, cubic AgBr and rhombohedral $Bi_6O_5(OH)_3(NO_3)_5\cdot 2H_2O$ have been proved to form in the final product.

Microstructure and composition analyses

The microstructure of the as-prepared product was characterized by the TEM images, as shown in Fig. 2(a)–(c). In Fig. 2(a), it is observed that a large amount of AgBr NPs with diameters of 3–15 nm are uniformly dispersed on 6535BBN NSs. In Fig. 2(b) and (c), further observations at a high magnification reveals that some NPs distributed on NSs have sharp outlines, which indicates the loading of particles on the surface of NSs. Other particles are not easily distinguished, which suggests that these particles are sandwiched inside the curled or overlapped NSs. Fig. 2(c) shows that some NSs are curled or overlapped. To confirm its composition, EDS measurements were performed. Fig. 2(d) shows the EDS elemental mappings of the composite, which indicate the uniform distribution of the Bi, Ag, Br, N, and O elements. The EDS spectrum in Fig. 2(f) confirms the presence of these elements in the composite again. The crystalline nature of the product was analyzed by the SAED pattern, as shown in Fig. 2(e). Most of the diffraction rings are indexed to the crystalline planes of cubic AgBr (JCPDS no. 06-0438), including (200), (220), (311), (400), (331), (420), (440), (600), and (640). Other diffraction rings are aligned to the crystalline planes of rhombohedral $Bi_6O_5(OH)_3(NO_3)_5\cdot 2H_2O$ (JCPDS no. 54-0627), including (006), (226), (440), and (544). Based on the above analyses, it is concluded that the as-prepared product is composed of $Bi_6O_5(OH)_3(NO_3)_5\cdot 2H_2O$ and AgBr, which is consistent with the above XRD spectrum. The 6535BBN/AgBr composite has a typical LOC structure, where AgBr NPs is sandwiched in 6535BBN·$2H_2O$ NSs or loaded on their surfaces. The advantageous structure is expected to enhance the stability of AgBr particles and protect them from aggregation, which might prolong the antibacterial performance.

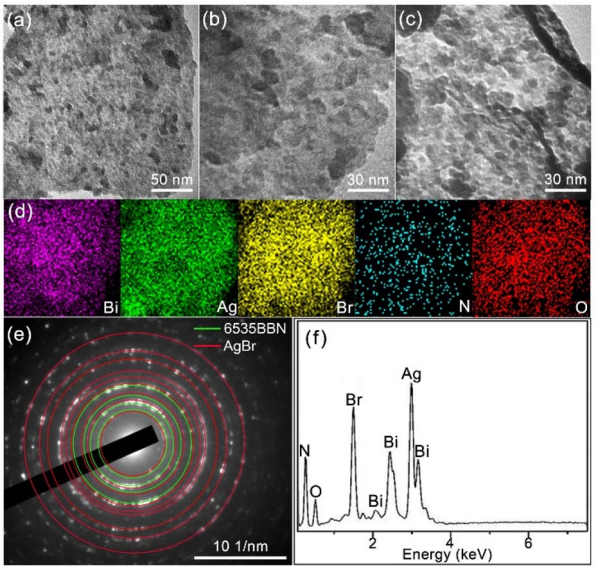

Fig. 2 (a–c) TEM images of the 6535BBN/AgBr composite; (d) EDS elemental mapping images of Bi, Ag, Br, N, and O elements; (e) SAED pattern of the composite; (f) EDS spectrum of the composite.

FTIR analysis

FTIR spectra were recorded to detect the functional groups on the surface of the as-prepared 6535BBN/AgBr composite. In the

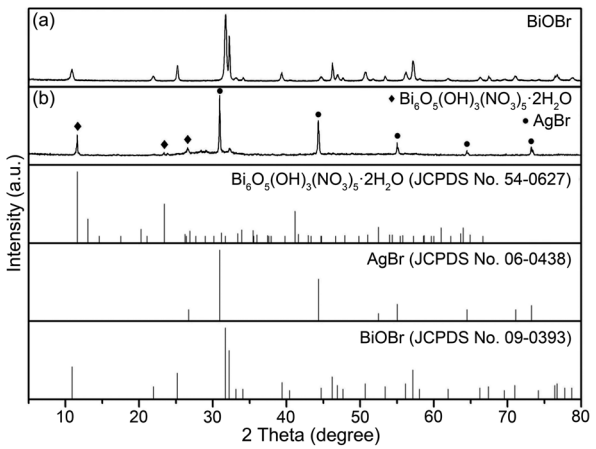

Fig. 1 XRD spectra of BiOBr (a) and 6535BBN/AgBr (b).

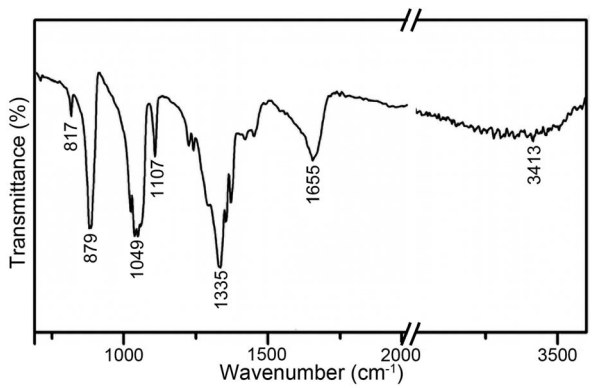

Fig. 3 FTIR spectrum of the 6535BBN/AgBr composite.

FTIR spectrum (Fig. 3), obvious adsorption bands at 817 cm^{-1}, 879 cm^{-1}, 1049 cm^{-1}, 1107 cm^{-1}, 1335 cm^{-1}, and 1655 cm^{-1} are detected. The peaks at 817 and 879 cm^{-1} are assigned to bending bands of NO_3^- groups.[40,41] The peaks at 1049 and 1107 cm^{-1} are related to symmetric stretching and bending vibrations of NO_3^- groups, respectively.[40,42] The strong peak at 1335 cm^{-1} is attributed to the asymmetric stretching vibration of NO_3^- groups.[40] Meanwhile, the weak peak at 1655 cm^{-1} might be due to the bending mode of water molecule and –OH.[43,44] In addition, a weak and broad absorption band (3000–3600 cm^{-1}) centered at 3413 cm^{-1} is related to the stretching vibrations of hydroxyl groups, physically adsorbed water, and crystal water.[40] In summary, most peaks in the FTIR spectrum are assigned to NO_3^- groups, which confirms the existence of NO_3^- in the composite and suggests the formation of $Bi_6O_5(OH)_3(NO_3)_5 \cdot 2H_2O$.

XPS measurements

The elemental composition and chemical status of 6535BBN/AgBr composite were determined by XPS measurements. In Fig. 4, the XPS survey spectrum of the composite and high-resolution spectra of Ag 3d, Br 3d, Bi 4f, N 1s, and O 1s are displayed. The survey spectrum (Fig. 4(a)) indicates that the as-prepared composite consisted of Br, Ag, Bi, N, and O. Carbon peaks can be ascribed to the XPS technique itself. In Fig. 4(b), two peaks at 367.38 eV and 373.38 eV are respectively assigned to Ag $3d_{3/2}$ and Ag $3d_{5/2}$ of Ag^+ in AgBr.[45] In Fig. 4(c), two peaks at 67.9 eV and 68.8 eV are associated with Br $3d_{5/2}$ and Br $3d_{3/2}$ of Br^- in AgBr.[45] In Fig. 4(d), two peaks at 159.3 eV and 164.6 eV are indexed to Bi $4f_{5/2}$ and Bi $4f_{7/2}$, which are characteristics of trivalent bismuth.[46] In Fig. 4(e), the peak at 406.55 eV is indexed to the binding energy of nitrogen in the NO_3^- anion of 6535BBN.[47] In Fig. 4(f), the peaks at 529.3 eV, 530.1 eV, 531.4 eV, and 532.2 eV are respectively matched to $[Bi_2O_2]^{2+}$, hydroxyl groups, crystal water, and N–O in $Bi_6O_5(OH)_3(NO_3)_5 \cdot 2H_2O$.[44,45] In conclusion, the above XPS spectra further indicates the formation of AgBr and 6535BBN in the composite, which is consistent with the above XRD, SAED, EDS, and FTIR analyses.

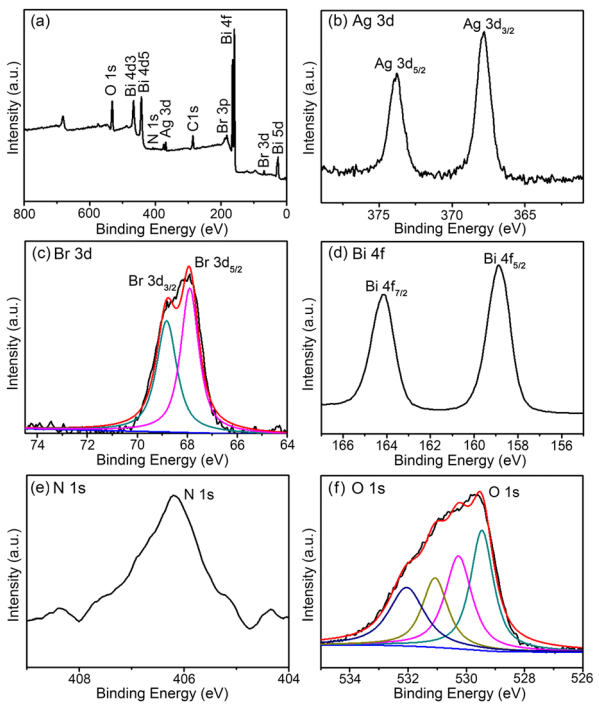

Fig. 4 (a) XPS survey spectrum of the 6535BBN/AgBr composite; (b–f) XPS high resolution spectra of Ag 3d, Br 3d, Bi 4f, N 1s, and O 1s.

Evaluation of long-lasting antibacterial efficacy

To evaluate the long-lasting antibacterial efficacy of 6535BBN/AgBr, the antibacterial activities of the composite after storage in water or 0.9% NaCl were tested. For comparison, the antibacterial activity of commercial AgBr after storage was tested under the same experimental conditions. The variation of antibacterial abilities with the storage time is represented by the corresponding inhibition zones against *E. coli*. As shown in Fig. 5(a)–(d), the diameters of the inhibition zones of pure AgBr stored in water for 0 h, 8 h, 16 h, and 48 h were respectively determined to be 21.06, 13.86, 6, and 6 mm, which displays a rapid decrease in the antibacterial activity. Diameters corresponding to the 6535BBN/AgBr composite stored in water for 0 h, 8 h, 16 h, and 48 h are 22.50, 21.71, 20.43, and 20.29 mm, respectively. The antibacterial activity of 6535BBN/AgBr after storage for 48 h remains 90.2% of that in the beginning, which exhibits the long-lasting antibacterial efficacy. The long-lasting activity might be suggested by the excellent stability and dispersion of powders in water. Fig. 5(e) and (f) display the digital images of 6535BBN/AgBr and AgBr solutions in transparent tubes, which were kept for 0 h, 8 h, 16 h, and 48 h without shaking. It is observed that 6535BBN/AgBr powders are well dispersed in water after storage for 48 h and remain turbid, while pure AgBr powders aggregate in water even after a short time. For AgBr powders in water, the aggregation in several hours is reversible. When the tube is shaken, the solution can return to turbid. After storage for 8 h, the aggregation of AgBr powders becomes irreversible and the precipitate is formed at the bottom of the tubes, which is consistent with the variation trends of inhibition zones diameters of AgBr after storage. Therefore, it is revealed that 6535BBN/AgBr powders in water

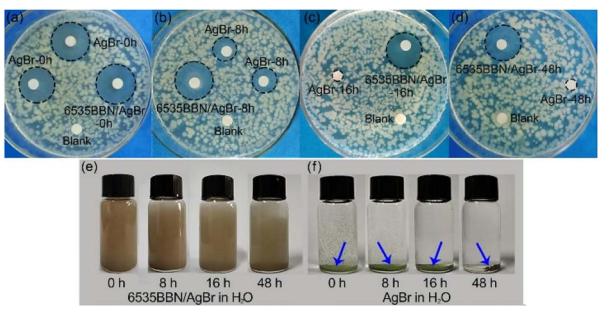

Fig. 5 (a–d) Inhibition zones of 6535BBN/AgBr and AgBr stored in water for 0 h, 8 h, 16 h, and 48 h; (e) digital images of 1 mg mL^{-1} 6535BBN/AgBr in water; (f) digital images of 10 mg mL^{-1} of AgBr in water.

are much more stable and resistant to aggregation compared to pure AgBr. The positive relationship between the dispersion state and long-lasting antibacterial performance is clarified.

For the purpose of exploring the potential value of 6535BBN/AgBr in clinical applications, the long-lasting antibacterial activity of the composite stored in 0.9% NaCl was measured. As shown in Fig. 6(a)–(c), the inhibition zone diameters corresponding to AgBr stored in 0.9% NaCl for 0 h, 8 h, and 16 h were respectively determined to be 13.07, 7.86, and 6 mm, which indicates the obvious decrease in the antibacterial activity in a short time. For comparison, the inhibition zone diameters corresponding to the 6535BBN/AgBr composite stored for 0 h, 8 h, and 16 h were 21.42, 19.57, and 19.29 mm, respectively. The antibacterial activity of 6535BBN/AgBr after storage for 16 h was determined to be 90.1% of that in the beginning. Thus, the long-lasting antibacterial activity of 6535BBN/AgBr stored in 0.9% NaCl is also revealed, although the time is shorter than that in water. The dispersion of pure AgBr and 6535BBN/AgBr powders in 0.9% NaCl are shown in Fig. 6(d) and (e). It is revealed that 6535BBN/AgBr powders are dispersed nearly uniformly in 0.9% NaCl after being stored for 16 h, while AgBr powders aggregate and precipitate quickly. The positive relationship between the improved dispersion state of 6535BBN/AgBr and its long-lasting antibacterial activity is represented again. For AgBr in 0.9% NaCl, the aggregation in several hours becomes irreversible and the precipitate is formed, which is consistent with the quick decrease in the diameters of the corresponding inhibition zones given in Fig. 6(a) and (b). To summarize, the employment of 6535BBN as carriers successfully endows the composite with long-lasting antibacterial efficacy in water or 0.9% NaCl, which might be attributed to the advantageous LOC structure in the composite.

Mechanism of long-lasting antibacterial efficacy

In general, the antibacterial activity of 6535BBN/AgBr is attributed to the distinct antibacterial capacity of BBN, ROS antibacterial action, and silver ions' sterilization. BBN compounds exhibit antibacterial capacities as inhibiting enzymes and delaying bacterial growth.[35] ROS produced by photocatalytic actions might cause the loss of membrane structure and functions, which leads to cell wall lysis and final disruption of bacteria.[11,15,16] The silver ions released from AgBr penetrate the membrane and react with the sulfhydryl group on the bacterial protein. Bacteria are inactivated due to the coagulation of proteins and the disability of synthase.[13,14] In our study, 6535BBN is combined with AgBr by a typical LOC structure, where the steady distribution of AgBr NPs with decreased size on 6535BBN NSs is realized. In comparison with bulk BBN in the microscale,[38] distinct antibacterial capacity of 6535BBN NSs might be improved due to much more contact between the nanosheets with the bacteria. Before antibacterial actions, the adhesion of the bacteria might be strengthened due to the size decrease of BBN sheets and AgBr particles.

Due to the construction of the LOC structure, the long-lasting efficacy of 6535BBN/AgBr is promoted by the synergy of three effects, as illustrated in Fig. 7. Firstly, the blade-like edges of 6535BBN NSs might exert physical damage to bacterial cells, which cause cytoplasm leakage, destruction of cellular integrity, and bacterial apoptosis. Secondly, the steady distribution of AgBr NPs on 6535BBN NSs protects AgBr from aggregation, which might prevent the quick release of Ag^+ and react with bacteria in external solution. The 6535BBN/AgBr nanocomposite is accepted as a sustainable resource of Ag^+, which controls the release rate of silver ions. Therefore, the release period of Ag^+ is extended and the sterilization effect is prolonged. Thirdly, ROS production based on photocatalysis is controlled because some AgBr NPs are sandwiched in BBN NSs. But the ROS total amount might be elevated due to the improved production and utilization efficiencies of photogenerated carriers. The size decrease of BBN sheets and AgBr particles might enlarge the light absorption and improve the production of carriers. The movement of carriers from interior to the surface is accelerated and their utilization rate is improved. The separation of carriers might be promoted by their efficient transfer through the interfaces in the nanoscale between AgBr and BBN. Therefore, the slow production of more

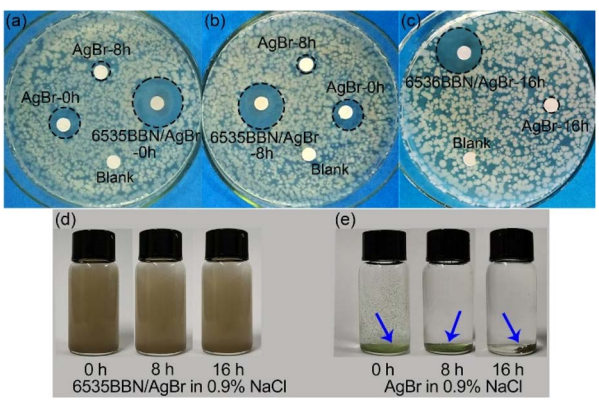

Fig. 6 (a–c) Inhibition zones of 6535BBN/AgBr and AgBr stored in 0.9% NaCl for 0 h, 8 h, and 16 h; (d) digital images of 1 mg mL^{-1} 6535BBN/AgBr in 0.9% NaCl; (e) digital images of 10 mg mL^{-1} of AgBr in 0.9% NaCl.

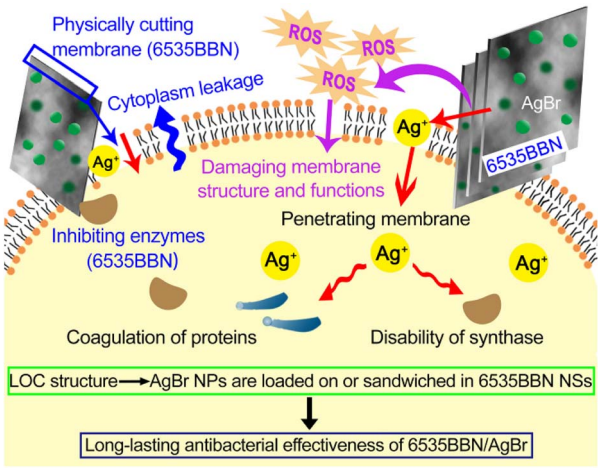

Fig. 7 Mechanism of long-lasting antibacterial efficacy of the 6535BBN/AgBr composite.

ROS enhances the long-acting antibacterial effect. In summary, long-lasting antibacterial efficacy of 6535BBN/AgBr is attributed to the sharp-edge-cutting effect of 6535BBN NSs, restrained sterilization effects of Ag^+ caused by their slow release, and prolonged ROS antibacterial effect caused by the slow production of more ROS. The sharp edges of BBN NSs damage the bacterial cell membranes, physically making Ag^+ and ROS penetrate into the cells and react with the bacterial cell more conveniently. The prominent long-lasing antibacterial activity of 6535BBN NSs endows it with expectable practical value for clinical applications.

Conclusion

The 6535BBN/AgBr nanocomposite exhibits long-lasting antibacterial efficacy against *E. coli*. The antibacterial performance of the composite after storage for different durations was assessed by the inhibition zones. It is indicated that the activities of the composite after storage for 48 h in water and 16 h in 0.9% NaCl remains 90.2% and 90.1% of that in the beginning, respectively. The time of antibacterial efficacy of the composite stored in 0.9% NaCl is shorter than that in water. The long-lasting antibacterial activities are suggested by the excellent dispersion of the composite powders in the solutions. It is revealed that 6535BBN/AgBr powders are dispersed nearly uniformly in 0.9% NaCl or water after storage, while AgBr powders aggregate and precipitate quickly even after a short time. The LOC structure of the composite had AgBr NPs sandwiched in 6535BBN NSs or loaded on their surfaces, which contributes to its long-lasting antibacterial performance. The mechanism of the long-lasting efficacy is discussed based on the sharp-edge-cutting effect of 6535BBN NSs, restrained sterilization effects of silver ions, and prolonged ROS antibacterial effect. The stable 6535BBN/AgBr composite with long-term antibacterial activity provides an efficient strategy to overcome the bacterial resistance in practical clinical applications.

Author contributions

Mei Zhao: investigation, writing – original draft; Mengchen Liu: formal analysis & software, writing – review & editing; JinFeng Yao: software, writing – review & editing; Wenyu Li: writing – review & editing; Chengdong Li: writing – review & editing; Qian Zhang: software; Zhihua Zhang: investigation, supervision; Wenjun Wang: writing – review & editing.

Conflicts of interest

The authors declare that they have no known competing financial interests or personal relationships that could have appeared to influence the work reported in this paper.

Acknowledgements

This work was sponsored by National Natural Science Foundation of China under Grant No. 51672145, 52171229, and 51872034.

Notes and references

1 X. Y. Chen, X. Peng, L. B. Jiang, X. Z. Yuan, J. Fei and W. Zhang, *Chem. Eng. J.*, 2022, **427**, 130945.
2 C. W. Du, S. Y. Nie, C. Zhang, T. Wang, S. Z. Wang, J. Zhang, C. F. Yu, Z. S. Lu, S. Y. Dong, J. L. Feng, H. J. Liu and J. H. Sun, *J. Colloid Interface Sci.*, 2022, **606**, 1715–1728.
3 X. Yang, H. Sun, S. K. Maddili, S. Li, R. G. Yang and C. H. Zhou, *Eur. J. Med. Chem.*, 2022, **232**, 114188.
4 M. N. Fan, J. X. Si, X. G. Xu, L. F. Chen, J. P. Chen, C. Yang, J. W. Zhu, L. H. Wu, J. Tian, X. Y. Chen, X. Z. Mou and X. J. Cai, *Carbohydr. Polym.*, 2021, **257**, 117636.
5 X. X. Wu, Y. Zhang, T. Hu, W. X. Li, Z. L. Li, H. J. Hu, S. R. Zhu, W. Z. Chen, C. S. Zhou and G. B. Jiang, *Int. J. Biol. Macromol.*, 2021, **167**, 1211–1220.
6 Z. W. Jian, H. Wang, M. L. Liu, S. Y. Chen, Z. H. Wang, W. Qian, G. X. Luo and H. S. Xia, *Mater. Sci. Eng., C*, 2020, **111**, 110833.
7 F. Gao, H. J. Zhou, Z. C. Shen, G. W. Zhu, L. Hao, H. Y. Chen, H. Xu and X. H. Zhou, *Colloids Surf., B*, 2020, **188**, 110784.
8 T. Liang, Y. P. Wang, L. L. Zeng, Y. Z. Liu, L. P. Qiao, S. F. Zhang, R. F. Zhao, G. Q. Li, R. F. Zhang, J. H. Xiang, F. C. Xiong, A. Shanaghi, H. B. Pan and Y. Zhao, *Appl. Surf. Sci.*, 2020, **509**, 144717.
9 Y. Sugiura, F. Ono, M. Nohara, R. Horino, K. Kutara, T. Kanda, K. Oowada, M. Horie and Y. Makita, *Mater. Today Commun.*, 2022, **30**, 103130.
10 L. Ye, Z. M. Cao, X. M. Liu, Z. D. Cui, Z. Y. Li, Y. Q. Liang, S. L. Zhu and S. L. Wu, *J. Alloys Compd.*, 2022, **904**, 164091.
11 R. Wang, M. S. Shi, F. Y. Xu, Y. Qiu, P. Zhang, K. L. Shen, Q. Zhao, J. G. Yu and Y. F. Zhang, *Nat. Commun.*, 2020, **11**, 4465.
12 W. X. Liu, Z. F. Tao, D. Wang, Q. Q. Liu, Y. N. Zhang, Y. L. Zhang and A. Dong, *J. Hazard. Mater.*, 2020, **410**, 124601.
13 F. F. Liu, X. W. Cheng, L. Xiao, Q. Wang, K. Yan, Z. Su, L. Wang, C. Ma and Y. B. Wang, *Int. J. Biol. Macromol.*, 2021, **167**, 1338–1348.
14 W. X. Fang, S. H. Ma, H. Dong, X. W. Jin, Y. C. Zou, K. X. Xu, L. Zhang and Y. H. Luo, *ACS Appl. Nano Mater.*, 2021, **4**, 5541–5547.
15 A. Balapure, Y. Nikhariya, N. S. S. Boppudi, R. Ganesan and J. R. Dutta, *ACS Appl. Mater. Interfaces*, 2020, **12**, 21481–21493.
16 M. Sboui, S. Bouattour, M. Gruttadauria, G. Marcì, L. F. Liottaand and S. Boufi, *Nanomaterials*, 2020, **10**, 470.
17 C. F. Chen, D. Y. Wang, Y. N. Li, H. Y. Huang and Y. C. Ke, *Appl. Surf. Sci.*, 2021, **565**, 150534.
18 M. Padervand, M. R. Elahifard, R. V. Meidanshahi, S. Ghasemi, S. Haghighi and M. R. Gholami, *Mater. Sci. Semicond. Process.*, 2012, **15**, 73–79.
19 S. P. Pasaribu, M. Ginting, I. Masmur, J. Kaban and Hestina, *J. Mol. Liq.*, 2020, **310**, 113263.
20 H. B. He, Z. Z. Luo and C. L. Yu, *Colloids Surf., A*, 2021, **613**, 126099.

21 Y. F. Zhan, J. W. Lan, J. J. Shang, L. Yang, X. M. Guan, W. X. Li, S. Q. Chen, Y. Qi and S. J. Lin, *J. Alloys Compd.*, 2020, **822**, 153579.
22 L. Svoboda, J. Bednářa, R. Dvorský, Z. Rybková, K. Malachová, J. Henych, D. Matýsek and Z. Němečková, *Appl. Surf. Sci.*, 2020, **529**, 147098.
23 D. Yuan, L. Y. Huang, Y. P. Li, H. Wang, X. Q. Xu, C. B. Wang and L. Yang, *Dyes Pigm.*, 2020, **177**, 108253.
24 Z. Kubasheva, M. Sprynskyy, V. R. Plugaru, P. Pomastowski, A. Ospanova and B. Buszewski, *Materials*, 2020, **13**, 3409.
25 T. B. Devi and M. Ahmaruzzaman, *J. Alloys Compd.*, 2021, **860**, 157988.
26 M. Z. Chamba, S. Rajendran, M. H. Robledo, A. K. Priya and C. N. Cardenas, *Environ. Res.*, 2022, **209**, 112834.
27 J. Liu, Y. Li, L. Huang, C. B. Wang, L. Yang, J. W. Liu, C. Y. Huang and Y. H. Song, *Appl. Surf. Sci.*, 2021, **567**, 150713.
28 M. K. d. N. S. Leandro, J. V. B. Moura, P. d. T. C. Freire, M. L. Vega, C. d. L. Lima and Á. A. Hidalgo, *Antibiotics*, 2021, **10**, 1068.
29 T. Deng, Y. Q. Jia, Z. W. Tong, J. R. Shi, Z. Q. Wang and Y. Liu, *Microbiol. Spectrum*, 2022, **10**, e01578-21.
30 S. H. Ma, X. Luo, G. Ran, Y. P. Li, Z. Q. Cao, X. Y. Liu, G. Q. Chen, J. H. Yan and L. Wang, *Chem. Eng. J.*, 2022, **435**, 134810.
31 H. J. Hu, Q. F. Han, H. Z. Liu, Z. C. Shen and H. P. Bi, *J. Mater. Sci.*, 2020, **55**, 11984–11998.
32 S. C. Sun, W. Xiao, C. T. You, W. M. Zhou, Z. N. Garba, L. W. Wang and Z. H. Yuan, *J. Cleaner Prod.*, 2021, **294**, 126350.
33 J. A. Oliveira, J. A. Torres, R. V. Gonçalves, C. Ribeiro, F. G. E. Nogueira and L. A. M. Ruotolo, *Mater. Res. Bull.*, 2021, **133**, 111073.
34 S. C. Sun, W. M. Zhou, L. Y. Wang, M. X. Zhang, I. Lawan, L. W. Wang, F. Zhang, M. Lin and Z. H. Yuan, *Int. J. Hydrogen Energy*, 2021, **46**, 25832–25842.
35 H. H. Jing, X. Q. Chen and X. Y. Jiang, *Micro Nano Lett.*, 2011, **6**, 196–200.
36 L. Miersch, M. Schlesinger, R. W. Troff, C. A. Schalley, T. Ruffer, H. Lang, D. Zahn and M. Mehring, *Chem. - Eur. J.*, 2011, **17**, 6985–6990.
37 T. A. Udalova, O. A. Logutenko, E. V. Timakova, L. I. Afonina, E. S. Naydenko and Y. M. Yukhin, *IFOST*, IEEE, 2008, pp. 137–140.
38 M. Zhao, X. X. Hou, L. Lv, Y. Y. Wang, C. D. Li and A. L. Meng, *Mater. Sci. Eng., C*, 2019, **98**, 83–88.
39 M. Zhao, Q. Yuan, H. Zhang, C. D. Li, Y. Y. Wang and W. J. Wang, *J. Alloys Compd.*, 2019, **782**, 1049–1057.
40 J. Y. Xiao, H. Zhang, Y. Xia, Z. L. Li and W. Huang, *RSC Adv.*, 2016, **6**, 39861–39869.
41 P. Vlazan and M. Stoia, *Ceram. Int.*, 2018, **4**, 530–536.
42 Z. N. Kayani, M. Umer, S. Riaz and S. Naseem, *J. Electron. Mater.*, 2015, **44**, 3704–3709.
43 K. Nejatia, H. Keypour, P. D. K. Nezhad, Z. Rezvani and K. A. Zeynali, *J. Taiwan Inst. Chem. Eng.*, 2015, **53**, 168–175.
44 Y. Q. Ouyang, Y. W. Xu, L. M. Zhao, M. Z. Deng, P. F. Yang, G. W. Peng and G. J. Ke, *Sci. Rep.*, 2021, **11**, 21625.
45 P. Zhang, Z. Y. Dong, Y. M. Ran, H. L. Xie, Y. Lu and S. M. Ding, *J. Mater. Res.*, 2018, **33**, 3953–3962.
46 J. W. Pang, Q. F. Han, W. Q. Liu, Z. C. Shen, X. Wang and J. W. Zhu, *Appl. Surf. Sci.*, 2017, **422**, 283–294.
47 X. M. Hu, L. J. Cheng and G. S. Li, *Mater. Lett.*, 2017, **203**, 77–80.